OPEN

NPG Asia Materials (2017) 9, e403; doi:10.1038/am.2017.78
www.nature.com/am

ORIGINAL ARTICLE

Platinum loaded on dual-doped TiO_2 as an active and durable oxygen reduction reaction catalyst

Bing-Jen Hsieh[1], Meng-Che Tsai[1], Chun-Jern Pan[1], Wei-Nien Su[2], John Rick[1], Jyh-Fu Lee[3], Yaw-Wen Yang[3] and Bing-Joe Hwang[1,3]

In this work, dual-doped TiO_2 was successfully synthesized by using tungsten or niobium as the cation and nitrogen as the anion and, as compared with single-doped TiO_2, provided a higher electron conductivity and improved physical properties. Platinum (Pt) nanoparticles loaded on these materials showed better electrochemical performance, and the $Pt/Ti_{0.9}Nb_{0.1}N_xO_y$ and $Pt/Ti_{0.8}W_{0.2}N_xO_y$ catalysts were 2.6–3.7 times more active than the $Pt/Ti_{0.9}Nb_{0.1}O_y$ and $Pt/Ti_{0.8}W_{0.2}O_y$ catalysts without nitrogen doping. Additionally, there was an activity loss of 22.9% as compared with 81% in Pt/C after 30 000 cyclic voltammetry cycles, a value exceeding the US Department of Energy (DOE) stability target. Dual doping not only enhances the electron conductivity but also changes the electronic state of Pt on the support materials, thus allowing for more active and stable catalysts. Both X-ray absorption spectroscopy (XAS) and density functional theory (DFT) studies were undertaken to demonstrate how defect formation affects the interactions between Pt and the single- or dual-doped TiO_2 supports and manipulates the physical and chemical properties of the resulting catalysts. Thus, these catalytic supports are strong candidates for proton exchange membrane fuel cell applications.

NPG Asia Materials (2017) **9,** e403; doi:10.1038/am.2017.78; published online 7 July 2017

INTRODUCTION

Fuel cells hold promise as highly efficient devices that directly convert fuels, such as hydrogen and oxygen, into water to produce electrical energy. Central to fuel cell operation is the proton exchange membrane, with its associated anodic and cathodic catalysts. Platinum (Pt), as a proton exchange membrane fuel cell catalyst, has the best performance among catalytic metals; however, the high cost of Pt and the lower reaction rate on the cathode, which is the site of the oxygen reduction reaction (ORR), limit the widespread use of proton exchange membrane fuel cells. Crucial to long-term fuel cell viability is the nature of the support used in the Pt catalyst. Graphitized-carbon supports can be used to replace carbon black, in forms such as nanotubes, nanofibers and graphene nanosheets, to improve chemical and electrochemical stability under the conditions within the fuel cell during the ORR. However, Pt sintering and support degradation remain unresolved problems in acid solutions.[1] One critical factor that underlies the corrosion of carbon supports, which ultimately leads to sintering and consequent aggregation/loss of catalytic metal nanoparticles, is the weak interaction between Pt and the carbon support.[2]

To improve catalyst durability, some researchers, including our group, have adopted the approach of replacing inherently unstable carbon supports with more robust and electrochemically stable metal oxide supports.[3–5] This latter approach, apart from providing the advantage of mechanical stability on the resulting catalytic structure, allows for the exploitation of strong metal-support interactions (SMSIs) that promote catalytic activity.[2] The most commonly used support (as a Pt carrier) is titanium dioxide, owing to its electrochemical stability and its resistance to dissolution in acidic media, as found in working fuel cells.

Although TiO_2 allows for some degree of electron transfer from Pt to the electrode, its conductivity is far lower than that of carbon. This decreased conductivity effectively limits the activity of Pt/TiO_2 catalysts, such that they are not comparable to Pt/C catalysts. One common approach to enhance the conductivity of TiO_2 and thus increase the activity of the catalyst is to dope other elements (cationic or anionic) into the TiO_2 lattice. Most previous studies have focused on single cation doping to enhance the conductivity of the TiO_2 support, using elements such as Nb,[6,7] Mo,[8,9] W,[10] Ru[2] or Ta.[11] In addition to increasing the conductivity, some researchers have found that doping can also enhance both the stability and SMSI by allowing the support to donate more electron density to Pt, thereby enhancing both catalyst durability and activity in the ORR.[8,9,11]

[1]Nanoelectrochemistry Laboratory, Department of Chemical Engineering, National Taiwan University of Science and Technology, Taipei, Taiwan; [2]Nanoelectrochemistry Laboratory, Graduate Institute of Applied Science and Technology, National Taiwan University of Science and Technology, Taipei, Taiwan and [3]National Synchrotron Radiation Research Center, Hsinchu, Taiwan
Correspondence: Professor W-N Su, Nanoelectrochemistry Laboratory, Graduate Institute of Applied Science and Technology, National Taiwan University of Science and Technology, 43, Keelung Road, Section 4, Taipei 106, Taiwan.
E-mail: wsu@mail.ntust.edu.tw
or Professor B-J Hwang, Nanoelectrochemistry Laboratory, Department of Chemical Engineering, National Taiwan University of Science and Technology, 43, Keelung Road, Section 4, Taipei 106, Taiwan.
E-mail: bjh@mail.ntust.edu.tw
Received 29 November 2016; revised 28 February 2017; accepted 24 March 2017

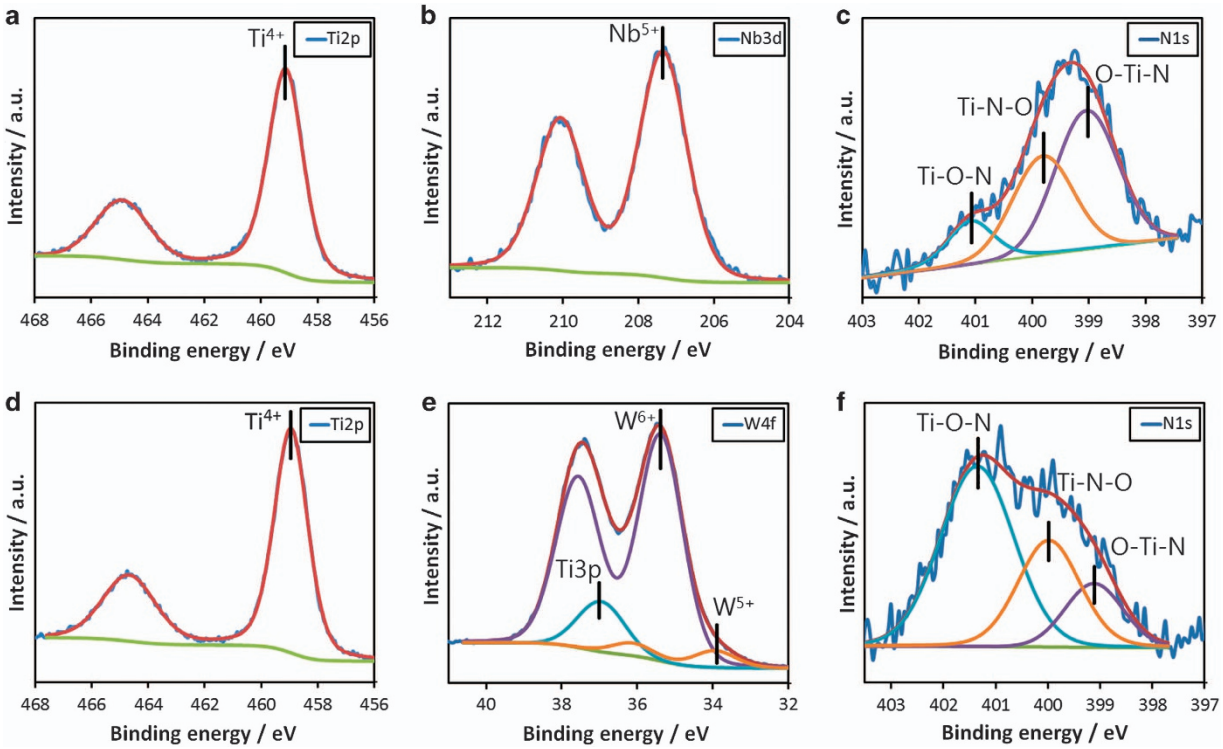

Figure 1 X-ray photoelectron spectroscopy spectra of (**a**) Ti 2p, (**b**) Nb 3d and (**c**) N 1s of $Ti_{0.9}Nb_{0.1}N_xO_y$. (**d**) Ti 2p, (**e**) W 4f and (**f**) N 1s of $Ti_{0.8}W_{0.2}N_xO_y$.

Anion (such as N or F)-doped TiO_2 has been used as a photocatalyst material.[12–14] The introduction of these dopants decreases the band gap of TiO_2 and thereby enhances both the electron conductivity and photocatalyst activity. In contrast to the many studies focused on anion doping in photocatalyst materials, few studies have investigated the use of anion-doped TiO_2 as a Pt catalyst support for fuel cell applications. In addition to single ion doping, the TiO_2 lattice can simultaneously accommodate both cationic and anionic dopants. This 'dual-doped' material provides a much lower bandgap than single-ion-doped TiO_2[15–17] and greater electron conductivity compared with that of single-doped materials. An intriguing question naturally arises as to the utility, application and activity of dual-doped supports for Pt catalysts in fuel cell applications.

In this study, electrochemical and spectroscopic data together with ORR activity studies indicated that $Ti_{0.9}Nb_{0.1}N_xO_y$ and $Ti_{0.8}W_{0.2}N_xO_y$ synthesized as dual-doped catalytic supports for Pt nanoparticles offer considerable promise as a new class of catalytic support for use in fuel cells. In conjunction with these experimental approaches, a computational density functional theory (DFT) study showing the differences in electron density distributions in different materials was undertaken to shed light on the mechanistic basis for the enhanced catalytic activity found in dual-doped materials.

MATERIALS AND METHODS

Dual-doped $Ti_{0.8}W_{0.2}N_xO_y$ and $Ti_{0.9}Nb_{0.1}N_xO_y$ supports were synthesized using a newly developed hydrothermal route in which 95% ethanol was used as the solvent. First, 95% ethanol (40 ml) was cooled to 5 °C, and then a calculated amount of titanium (IV) chloride ($TiCl_4$, ⩾99.0%) was introduced with continuous stirring. Second, a calculated amount of tungsten (VI) chloride (WCl_6, ⩾99.9%) or niobium (V) chloride ($NbCl_5$, ⩾99.9%) was dissolved by ultrasonication in absolute alcohol (2 ml, 99.5%) for several minutes. The tungsten or niobium precursor solution was then purged into the cooled 95% ethanol solution with continuous stirring. Urea (0.6 g, 99.0%) was dissolved in 95% ethanol (20 ml) and then mixed with the precursor solution. The resulting solution was stirred for 15 min and then transferred into a Teflon bottle that was then sealed in an autoclave reactor and heated to 150 °C (heating rate 10 °C min^{-1}) and maintained at this temperature for 2 h. The reactor was then allowed to cool to room temperature. The resulting $Ti_{0.8}W_{0.2}N_xO_y$ or $Ti_{0.9}Nb_{0.1}N_xO_y$ suspensions were centrifuged and washed with deionized water (16 500 r.p.m. for 10 min; 3 times). The material was dried at 80 °C for 12 h before platinization and characterization. For comparative purposes, TiO_2 nanoparticles doped with only tungsten, niobium or nitrogen were also synthesized without the addition of urea or metal chloride precursors using the same synthetic procedure.

Table 1 Electronic conductivities and BET (Brunauer–Emmett–Teller) surface areas

Samples	*Electronic conductivity* ($S\ cm^{-1}$)	*BET surface area* ($m^2\ g^{-1}$)	*Pore size center* (*nm*)
TiO_2	8.9×10^{-6}	50	
TiN_xO_y	5.5×10^{-3}	194	7.4
$Ti_{0.8}W_{0.2}O_y$	3.32×10^{-1}	115.6	3.6
$Ti_{0.8}W_{0.2}N_xO_y$	2.13	190.5	3.6
$Ti_{0.9}Nb_{0.1}O_y$	4.47×10^{-2}	178.6	6.3
$Ti_{0.9}Nb_{0.1}N_xO_y$	0.312	240.2	3.7

The catalytic structures were formed by loading Pt nanoparticles onto the metal oxide supports with a microwave technique.[2,8,9] The supporting nanoparticles ($Ti_{0.8}W_{0.2}N_xO_y$ or $Ti_{0.9}Nb_{0.1}N_xO_y$, 0.1 g) and ethylene glycol (20 ml, ⩾99.0%) were mixed in a 100- ml round-bottomed flask with magnetic stirring for 30 min. The suspension was ultrasonicated for 1 h to ensure complete dispersion in the solvent and then cooled to 5 °C in an ice bath. Simultaneously, H_2PtCl_6 (0.0664 g, ~40% Pt basis) was dissolved in 5 °C

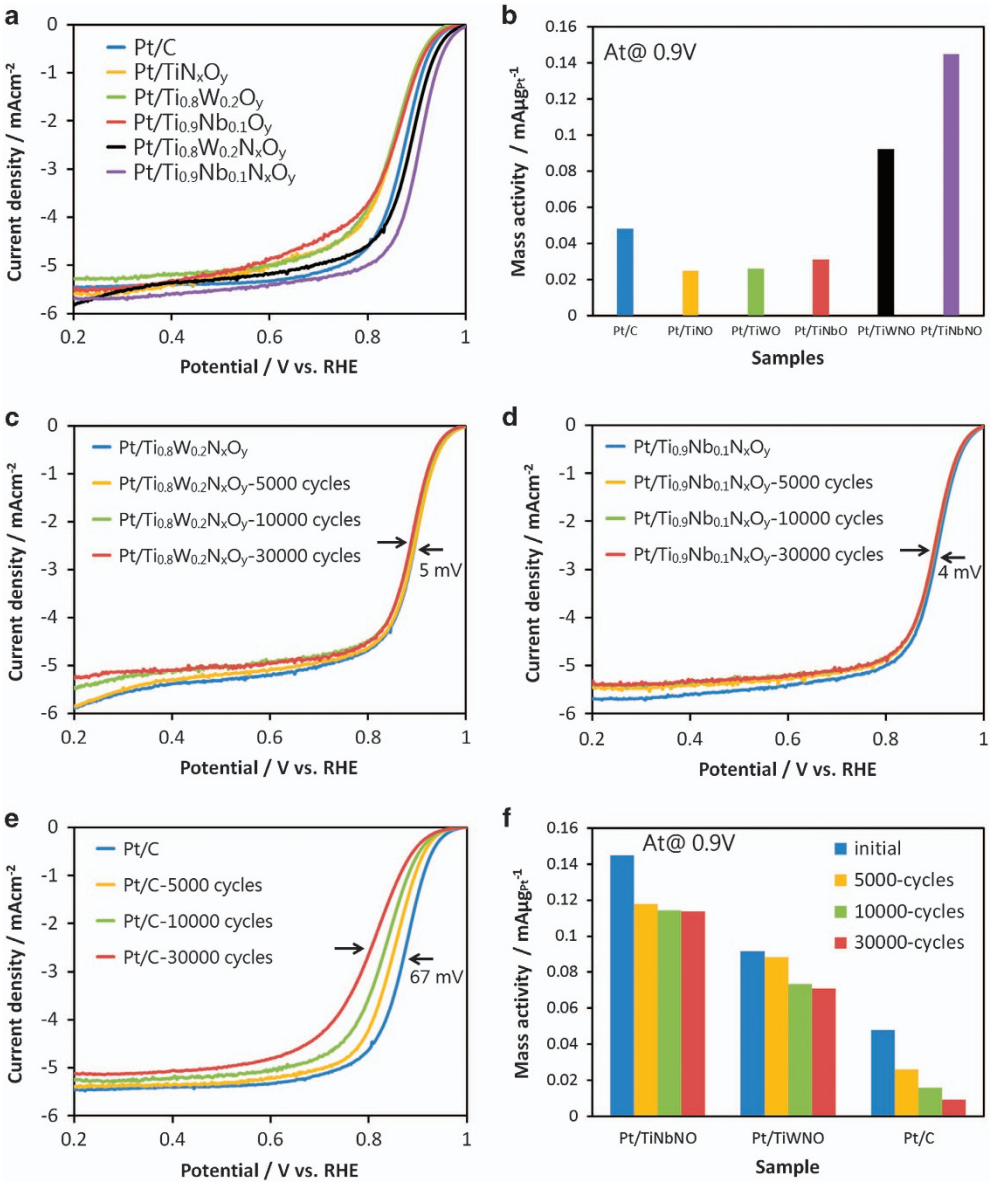

Figure 2 (**a**) Oxygen reduction reaction (ORR) polarization curves of Pt/C, Pt/TiN_xO_y, Pt/$Ti_{0.8}W_{0.2}O_y$, Pt/$Ti_{0.9}Nb_{0.1}O_y$, Pt/$Ti_{0.8}W_{0.2}N_xO_y$ and Pt/$Ti_{0.9}Nb_{0.1}N_xO_y$ catalysts. (**b**) Mass activity at 0.9 V vs reversible hydrogen electrode (RHE) (i_k). ORR polarization curves of (**c**) Pt/$Ti_{0.8}W_{0.2}N_xO_y$, (**d**) Pt/$Ti_{0.9}Nb_{0.1}N_xO_y$ and (**e**) Pt/C catalysts before and after 5000, 10 000 and 30 000 potential cycles. (**f**) Mass activity before and after stability testing at 0.9 V vs RHE (i_k).

ethylene glycol and formed an orange-colored, transparent solution. This solution was mixed into the previously prepared support suspension with continuous stirring for 30 min, and then 1 M NaOH was added to the ethylene glycol to adjust the pH to 11.5. The resulting yellow suspension was placed in a microwave oven (150 W) and heated to 160 °C for 2 min. After completion of the reaction, the sample was cooled to room temperature in air, and the resulting black precipitate was centrifuged and washed with acetone (3 times). The resulting 20 wt% Pt-loaded catalyst was oven dried (80 °C) for 12 h before characterization. Pt/TiN_xO_y, Pt/$Ti_{0.8}W_{0.2}O_y$ and Pt/$Ti_{0.9}Nb_{0.1}O_y$ were synthesized using the same procedure for comparison, and the Pt/C (20 wt%) reference was obtained from Johnson Matthey (London, UK). All the material characterizations and computational details are provided in the Supplementary Information.

RESULTS AND DISCUSSION

Dual-doped $Ti_{0.9}Nb_{0.1}N_xO_y$ and $Ti_{0.8}W_{0.2}N_xO_y$ were synthesized and characterized using X-ray photoelectron spectroscopy measurements to evaluate the chemical composition and bonding states (Figures 1a–f). The peak at 459.1 eV was assigned to Ti^{4+} of Ti 2p; the peaks at 35.4, and 33.9 eV were assigned to W^{6+} and W^{5+} of W 4f, respectively; the peak that overlapped with W 4f at 37 eV was assigned to Ti 3p and the peak at 207.4 eV was assigned to Nb^{5+}. Compared with the $Ti_{0.8}W_{0.2}O_y$ X-ray photoelectron spectroscopy result in Supplementary Figure S3, the X-ray photoelectron spectroscopy peaks of $Ti_{0.8}W_{0.2}N_xO_y$ for Ti 2p and W 4f slightly shifted to lower binding energies owing to doping with nitrogen that is less electronegative than oxygen.[18] The calculated Ti/W and Ti/Nb ratios (from the X-ray photoelectron spectroscopy data) were 78:22 and 89:11, respectively. The calculated N doping was 2.34 at% for $Ti_{0.9}Nb_{0.1}N_xO_y$ and 3.54 at% for $Ti_{0.8}W_{0.2}N_xO_y$. The peak at 399 eV was assigned to the N anion in the O–Ti–N bond[15,16,19]; the peak at 399.8 eV was assigned to interstitial doping (that is, Ti–N–O)[14,15,17] and the peak at 401.1 eV

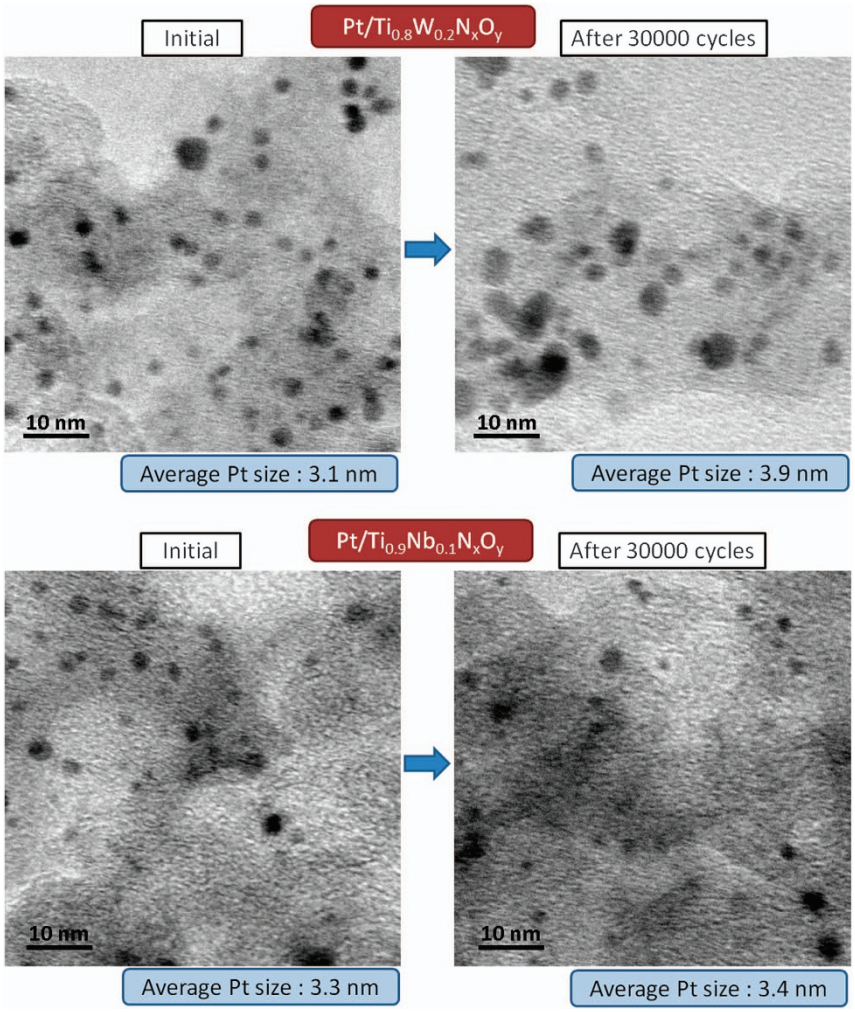

Figure 3 Transmission electron microscopy (TEM) images of $Pt/Ti_{0.8}W_{0.2}N_xO_y$ and $Pt/Ti_{0.9}Nb_{0.1}N_xO_y$ before and after 30 000 cyclic voltammetry (CV) cycles. (Inset) Size distribution of Pt nanoparticles.

was assigned to N ions in Ti–O–N linkages.[19] The different N 1s peak ratios at 399 and 401.1 eV between $Ti_{0.9}Nb_{0.1}N_xO_y$ and $Ti_{0.8}W_{0.2}N_xO_y$ indicated the presence of N ions in different structural environments. Although the complex binding in the dual-doped systems is still not clear, we demonstrated the successful hydrothermal synthesis of dual-doped TiO_2.

X-ray diffraction patterns were obtained to show the crystal structure of the dual-doped materials, and the results (Supplementary Figure S4) demonstrated that these two materials were homogeneous, thus indicating that after the synthesis procedure, the elements had uniformly formed a single-phase solid solution with the anatase-phase crystal structure.

To evaluate the conductivity difference between single-doped TiO_2 and dual-doped TiO_2, four-point probe electron conductivity measurements were conducted for both $Ti_{0.9}Nb_{0.1}N_xO_y$ and $Ti_{0.8}W_{0.2}N_xO_y$, and the conductivities of TiN_xO_y, $Ti_{0.9}Nb_{0.1}O_y$ and $Ti_{0.8}W_{0.2}O_y$ are listed for comparison in Table 1. For both $Ti_{0.9}Nb_{0.1}O_y$ and $Ti_{0.8}W_{0.2}O_y$, nitrogen doping further enhanced the conductivity. The synergetic effect of dual doping further decreased the band gap of single-ion-doped TiO_2,[15,20] thus resulting in a conductivity enhancement of another 6–7-fold.

The BET (Brunauer–Emmett–Teller) measurements for single-doped and dual-doped supports are shown in Supplementary Figure S5, and the numeric data of the BET surface areas are listed in Table 1. Both the $Ti_{0.9}Nb_{0.1}N_xO_y$ and $Ti_{0.8}W_{0.2}N_xO_y$ supports were mesoporous and had high surface areas (240.2 and 190.5 $m^2\,g^{-1}$, respectively) that were similar to that of the well-known Vulcan XC72 (232 $m^2\,g^{-1}$),[21] more than 4 times that of P25 TiO_2 (Degussa, 50 $m^2\,g^{-1}$) and higher than those of many dual-doped TiO_2 materials in photocatalyst studies.[16,20] The BET surface area results indicated that the dual-doped TiO_2 support surface area was sufficiently high to facilitate the dispersion of Pt nanoparticles.

Next, the Pt nanoparticles were loaded on the $Ti_{0.9}Nb_{0.1}N_xO_y$ and $Ti_{0.8}W_{0.2}N_xO_y$ supports for electrochemical testing. From the ORR polarization curves (Figure 2a), it was apparent that the half-wave potential, $E_{1/2}$, increased in the sequence: $Pt/TiN_xO_y < Pt/Ti_{0.8}W_{0.2}O_y < Pt/Ti_{0.9}Nb_{0.1}O_y < Pt/C < Pt/Ti_{0.8}W_{0.2}N_xO_y < Pt/Ti_{0.9}Nb_{0.1}N_xO_y$, thus revealing that the ORR activities of Pt on dual-doped TiO_2 were dramatically improved. The mass activities at 0.9 V (Figure 2b) were calculated on the basis of the ORR polarization curves and the Pt loading of the catalyst on the electrodes. The mass activity of $Pt/Ti_{0.8}W_{0.2}N_xO_y$ was ~3.6- and 3.7-fold greater than $Pt/Ti_{0.8}W_{0.2}O_y$, and Pt/TiN_xO_y, respectively, and almost twice that of the commercial Pt/C catalyst. An increase in catalyst activity was also observed with the $Pt/Ti_{0.9}Nb_{0.1}N_xO_y$ catalyst. The mass activity of

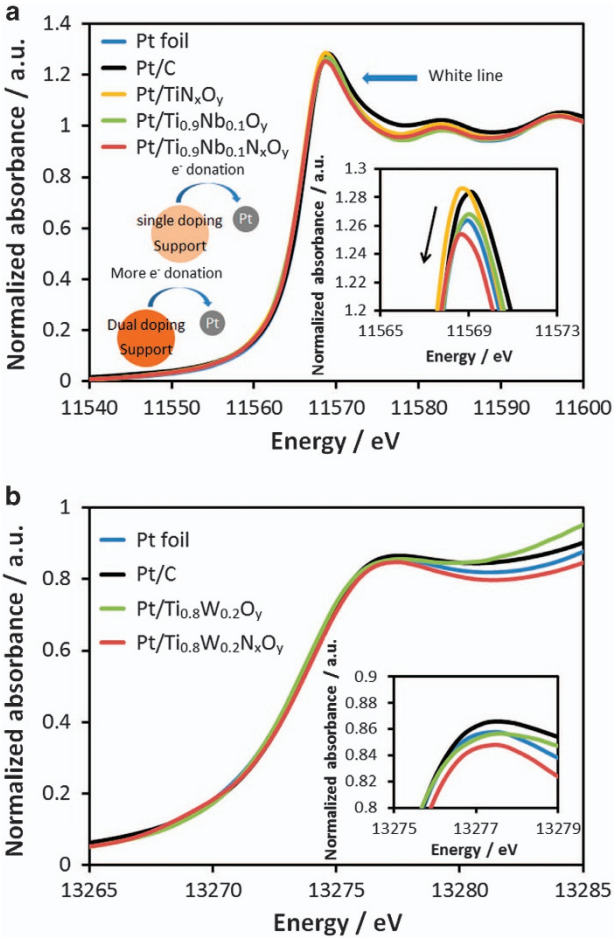

Figure 4 (**a**) Pt L_3-edge X-ray absorption near-edge spectroscopy (XANES) spectra of Pt/TiN_xO_y, $Pt/Ti_{0.9}Nb_{0.1}O_y$ and $Pt/Ti_{0.9}Nb_{0.1}N_xO_y$. Pt foil and Pt/C were measured as references. (Inset) Enlarged regions of the peaks of the Pt L_3-edge XANES white line. (**b**) Pt L_2-edge XANES spectra of $Pt/Ti_{0.8}W_{0.2}O_y$ and $Pt/Ti_{0.8}W_{0.2}N_xO_y$. Pt foil and Pt/C were measured as references. (Inset) Enlarged region of the peaks of the Pt L_2-edge.

$Pt/Ti_{0.9}Nb_{0.1}N_xO_y$ was ~4.7 and 5.8 times greater than $Pt/TiNb_{0.1}O_y$ and Pt/TiN_xO_y, respectively, and almost 3 times that of Pt/C. From the electrochemical results, it was apparent that both tungsten- and niobium-doped materials that were co-doped with nitrogen in TiO_2 showed an increase in the ORR activity that was greater than that of both nitrogen-doped and single cation-doped TiO_2. Similar to the conductivity results, the electrochemical tests also indicated the synergetic effect of dual-doped TiO_2.

Electrochemical stability tests were carried out at 25 °C, and the scanning range was between 0.6 and 1.0 V with a 50 mV s^{-1} scanning rate. ORR polarization curves of Pt/C, $Pt/Ti_{0.9}Nb_{0.1}N_xO_y$ and $Pt/Ti_{0.8}W_{0.2}N_xO_y$ were recorded after 5000, 10 000 and 30 000 cyclic voltammetry cycles in oxygen-saturated 0.1 M perchloric acid (Figures 2c–f). After the long-term stability tests, $Pt/Ti_{0.8}W_{0.2}N_xO_y$ showed only small changes in the ORR polarization curve. The half-wave potential only shifted ~1 mV after 5000 cycles and ~5 mV after 30 000 cycles. The mass activity loss in the $Pt/Ti_{0.8}W_{0.2}N_xO_y$ catalyst after 30 000 cycles was ~22.9%, a value far exceeding the US Department of Energy (DOE) 2017 fuel cell technical target of a mass activity loss <40% after 30 000 cycles between 0.60 and 1.0 V.[22] Similar results were observed for $Pt/Ti_{0.9}Nb_{0.1}N_xO_y$. The shifts in the half-wave potential of $Pt/Ti_{0.9}Nb_{0.1}N_xO_y$ after 5000 and 30 000 cycles were ~3 and ~4 mV, respectively, whereas the mass activity loss after 30 000 cycles was ~21.5%, a value also exceeding the DOE stability target. However, after 5000 cycles, the half-wave potential of Pt/C shifted ~24 mV, and the ORR activity was decreased by ~46%, and after 30 000 cycles, the half-wave potential shifted ~67 mV, and the ORR activity was decreased by ~81%. The severe loss of activity may have been due to carbon corrosion and Pt nanoparticle agglomeration on the carbon support.[23] Carbon oxidation and the weak interactions between the carbon support and the Pt nanoparticles cannot prevent the sintering or detachment of the Pt nanoparticles that results in a decrease in catalytic activity after long-term operation. However, dual-doped TiO_2 showed insignificant dissolution or corrosion in an acidic environment during the ORR. Figure 3 shows transmission electron microscopy images of the two catalysts, $Pt/Ti_{0.8}W_{0.2}N_xO_y$ and $Pt/Ti_{0.9}Nb_{0.1}N_xO_y$, before and after 30 000-cycle stability tests. Although several Pt nanoparticle aggregations occurred after long cyclic voltammetry cycles, the average particle size remained primarily unchanged. The results demonstrated the high stability of the oxide supports during the ORR and, as demonstrated in previous studies, SMSI may prevent the detachment or agglomeration of Pt nanoparticles.[8,9,11] To understand the origin of the enormous enhancements in activity and stability that resulted from dual-ion doping, as well as the interactions between Pt and the doped TiO_2 support, we used a combination of X-ray absorption spectroscopy (XAS) and DFT computation methods.

To investigate the electronic properties of Pt nanoparticles on $Ti_{0.9}Nb_{0.1}N_xO_y$ and to verify the SMSI state, Pt L_3-edge X-ray absorption near-edge spectroscopy was used. The spectrum was plotted and compared with those of the Pt/TiN_xO_y and $Pt/Ti_{0.9}Nb_{0.1}O_y$ catalysts, and Pt foil and Pt/C were measured as references (Figure 4a). In X-ray absorption near-edge spectroscopy, the intensity of the white line is a direct measure of the d-band vacancy. The decrease in the white-line intensity can be attributed to SMSIs that in turn lead to the electron transfer from the support to Pt. Additionally, the SMSIs decrease the adsorption strength of the oxygen intermediates that are formed during the ORR on the Pt surface in the rate determining step, thus leading to a faster reaction rate of the oxygen reduction reaction.[8] Another important effect of the SMSI is the enhancement of the bonding strength between Pt and the metal oxide support that prevents the migration and aggregation of Pt on the support's surface in long-term stability tests.[8,9,11] Surprisingly, the white-line intensity decreased in the following order: $Pt/TiN_xO_y > Pt/C > Pt/Ti_{0.9}Nb_{0.1}O_y >$ Pt foil $> Pt/Ti_{0.9}Nb_{0.1}N_xO_y$. The results of the calculation of the unfilled d-states also showed a similar tendency (Supplementary Figure S6). Here, $Pt/Ti_{0.9}Nb_{0.1}N_xO_y$ represented the lowest white-line intensity, thus indicating that dual-doped TiO_2 has a stronger metal-support interaction with Pt nanoparticles, thereby leading to higher activity and stability during electrochemical testing.

$Pt/Ti_{0.8}W_{0.2}N_xO_y$ was also compared with single-doped TiO_2. Owing to the Pt L_3-edge overlap with the W L_2-edge, only the Pt L_2-edge of the Pt foil, Pt/C, $Pt/Ti_{0.8}W_{0.2}O_y$ and $Pt/Ti_{0.8}W_{0.2}N_xO_y$ was measured (Figure 4b). $Pt/Ti_{0.8}W_{0.2}N_xO_y$ showed the lowest intensity of the Pt L_2-edge, thus indicating a strong driving force for electron transfer from the support to Pt because of the SMSI. Interestingly, compared with Pt/C, both $Pt/Ti_{0.9}Nb_{0.1}O_y$ and $Pt/Ti_{0.8}W_{0.2}O_y$ demonstrated electron donation from the support to Pt, but Pt/TiN_xO_y did not. This phenomenon was further investigated by using DFT computations.

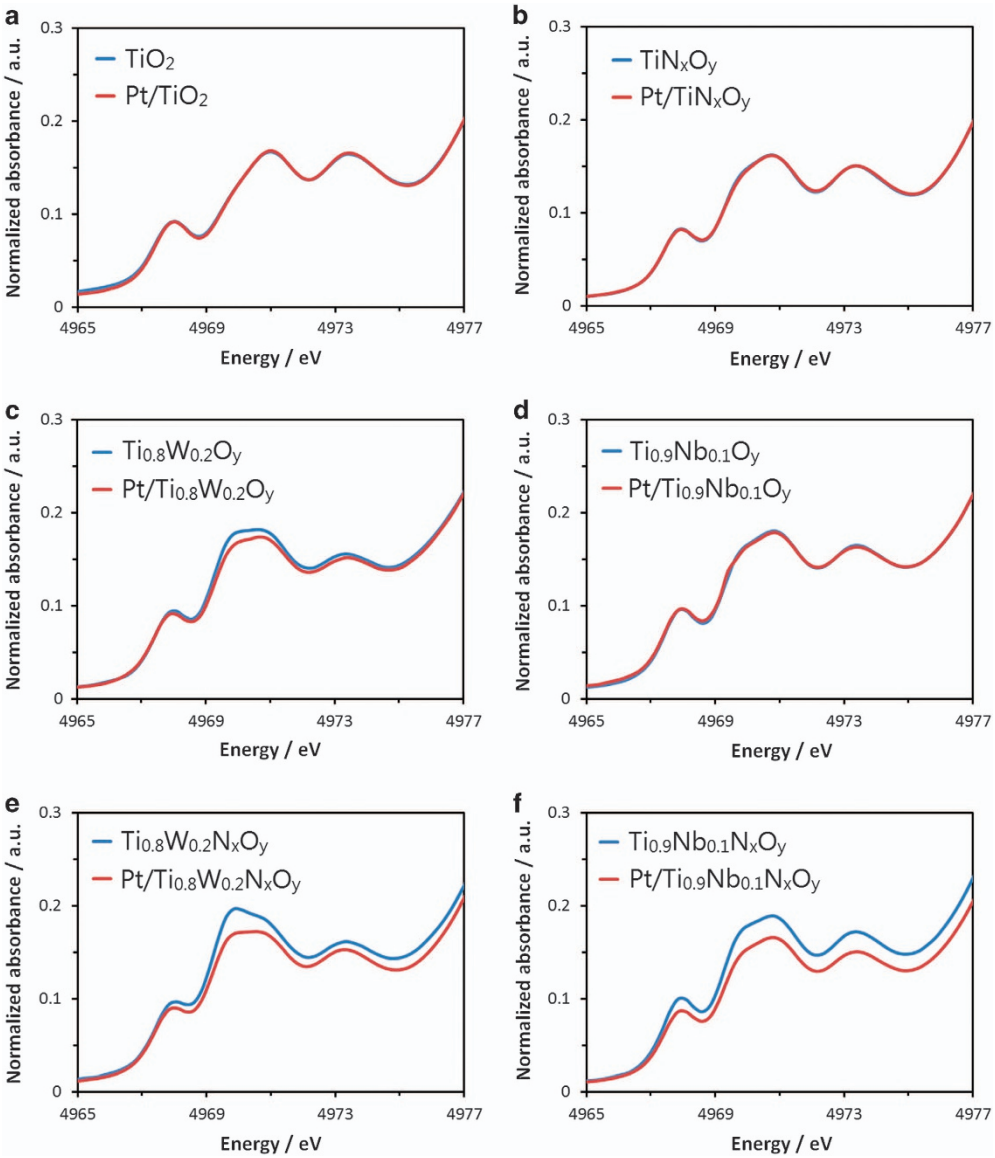

Figure 5 Ti K-edge X-ray absorption near-edge spectroscopy (XANES) spectra pre-edge region of (**a**) TiO_2 and Pt/TiO_2 (**b**) TiN_xO_y and Pt/TiN_xO_y, (**c**) $Ti_{0.8}W_{0.2}O_y$ and $Pt/Ti_{0.8}W_{0.2}O_y$, (**d**) $Ti_{0.9}Nb_{0.1}O_y$ and $Pt/Ti_{0.9}Nb_{0.1}O_y$, (**e**) $Ti_{0.8}W_{0.2}N_xO_y$ and $Pt/Ti_{0.8}W_{0.2}N_xO_y$ and (**f**) $Ti_{0.9}Nb_{0.1}N_xO_y$ and $Pt/Ti_{0.9}Nb_{0.1}N_xO_y$.

In the Supplementary Information, DFT calculations were used to examine the formation energy of the oxygen vacancy, the electronic state of Pt and bonding between Pt and the supports, and also to show the effect of doping in TiO_2-based supports on the physical and chemical properties of the catalysts. Supplementary Figure S9 shows the bonding strength of supported Pt (E_{1Pt}), valence electron variations in the deposited Pt ($\Delta\delta_{Pt}$) and E_{Ovac} (oxygen vacancy formation energy). These computational results exhibited the properties of Pt deposited on single-doped and dual-doped TiO_2 in the oxide support. Defects played an important role and significantly changed the properties of the deposited Pt. As shown in Supplementary Figure S9, Pt nanoparticles were found to be preferentially located at defect sites on most TiO_2-based supports and to gain electrons from it. This phenomenon induced an SMSI that enhanced both the activity and stability of Pt. From the XAS results, the decrease in the white-line intensity indicated that Pt should be deposited at defect sites rather than at defect-free sites. To further confirm this result, XAS measurements for the Ti K-edge were taken for single-doped and dual-doped TiO_2 supports with or without loading of Pt nanoparticles, and the pre-edge regions were compared (Figure 5). The three pre-edge peaks were attributed to crystalline TiO_2, whose intensities were related to the symmetry of the crystal structure. A distortion and oxygen vacancies can cause an increase in the pre-edge intensity.[24,25] In pure TiO_2 and single-doped TiO_2, the pre-edge intensity remained unchanged after Pt loading. In dual-doped TiO_2, Pt loading caused a decrease in the pre-edge intensity. The distortion in the crystal structure was unchanged after the loading of Pt nanoparticles, but the number of oxygen vacancies decreased when Pt nanoparticles were deposited on the defect sites. This decrease in vacancies resulted in a decrease in the pre-edge intensity, thus indicating that more Pt nanoparticles are deposited at the defect sites of the dual-doped supports. To determine the related amount of occupied defect sites, the peak intensity of the Ti K pre-edge between 4969 and 4973 eV of the support material was divided by the peak intensity of the support

with Pt loading. The result, termed an 'occupied defect,' was compared with the activity and unfilled state in Figure 6. The tendency of the occupied defect was similar to the catalyst activity, thus revealing that the Pt deposited on the defect sites of the support resulted in greater electron transfer from the support to Pt and provided both superior activity and stability for Pt on dual-doped TiO_2 compared with single-doped TiO_2.

Notably, the bonding strength of Pt on a defect site of the TiO_2-based support was much stronger than that of Pt on a defect-free site, except for N-doped TiO_2. In Pt/N-doped TiO_2, the E_{1Pt} on the defect-free site was much stronger than that on the defect site, thus indicating that Pt bound to a defect-free site of N-doped TiO_2 is more stable and leads to a positive $\Delta\delta_{Pt}$. This result was consistent with the increase in white-line intensity in the XAS measurements and the Ti pre-edge results of TiN_xO_y and Pt/TiN_xO_y. Finally, the XAS and DFT results demonstrated that the formation of defects play a pivotal role in dual-doped TiO_2 supports. Additionally, these supports are strong candidates for catalyst supports in oxygen reduction reactions.

Figure 7 illustrates the catalyst morphology after Pt loading on various support materials. As synthesized, the single-doped and dual-doped TiO_2 supports contained a certain number of oxygen vacancies on the surface. Several oxygen vacancies were occupied by Pt nanoparticles after platinization. Compared with the Pt deposited on the oxygen sites, the Pt that was deposited on the oxygen vacancy sites was more electronegative and had fewer hydroxyl groups on the surface during the ORR, thus providing a stronger driving force and more active sites for the ORR. The experimental results demonstrated that Pt occupied more defects on the dual-doped TiO_2 surface, thus making it easier to conduct the oxygen reduction reaction, and resulted in higher activity than that of Pt on a single-doped TiO_2 support.

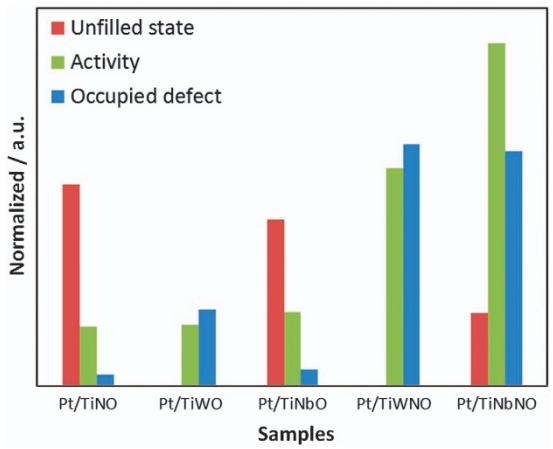

Figure 6 Normalized value of the unfilled state, activity and occupied defect of Pt/TiN_xO_y, $Pt/Ti_{0.8}W_{0.2}O_y$, $Pt/Ti_{0.9}Nb_{0.1}O_y$, $Pt/Ti_{0.8}W_{0.2}N_xO_y$ and $Pt/Ti_{0.9}Nb_{0.1}N_xO_y$ catalysts.

CONCLUSIONS

In this study, dual-doped TiO_2-supported Pt catalysts, which were prepared by an easy process and showed excellent activity and stability for oxygen reduction reactions, were developed. Dual-doped TiO_2 showed greater electron conductivity than did single ion-doped TiO_2. The BET results showed that the high surface area of $Ti_{0.9}Nb_{0.1}N_xO_y$ and $Ti_{0.8}W_{0.2}N_xO_y$ provided sufficient area for the improved dispersion of Pt nanoparticles. The electrochemical tests demonstrated that $Pt/Ti_{0.9}Nb_{0.1}N_xO_y$ and $Pt/Ti_{0.8}W_{0.2}N_xO_y$ had greater ORR activity than Pt/TiN_xO_y, $Pt/Ti_{0.9}Nb_{0.1}O_y$, $Pt/Ti_{0.8}W_{0.2}O_y$ and Pt/C catalysts. Additionally, both $Pt/Ti_{0.9}Nb_{0.1}N_xO_y$ and $Pt/Ti_{0.8}W_{0.2}N_xO_y$ showed high durability during stability testing. After 30 000 cyclic voltammetry cycles, the loss of activity for both catalysts was ˂22.9%, thus indicating better stability than that of a Pt/C catalyst and exceeding the stability target set by DOE. XAS measurements were carried out to identify the electronic properties of Pt on $Ti_{0.9}Nb_{0.1}N_xO_y$ and $Pt/Ti_{0.8}W_{0.2}N_xO_y$ supports. Combined with DFT studies, the results indicated that the high activity and stability is attributable to the SMSI between the Pt nanoparticles and affects the electron transfer from the support to Pt, thus leading to a faster catalytic reaction and the avoidance of Pt migration and sintering. Moreover, the results confirmed that the formation of defects on the support materials play an important role in the electron transfer phenomenon. The high electron conductivity of dual-doped TiO_2 may be another factor underlying the greater activity of $Pt/Ti_{0.9}Nb_{0.1}N_xO_y$ and $Pt/Ti_{0.8}W_{0.2}N_xO_y$ catalysts than Pt on single-doped TiO_2 for the ORR.

Finally, in principal, the anion–cation dual doping of TiO_2 is not limited to the use of nitrogen in combination with either niobium or tungsten, as explored here. Additional dual-doped TiO_2 supports may have applications in supporting catalytic metals other than Pt. This work opens a new path toward the development of new catalysts for fuel cell applications.

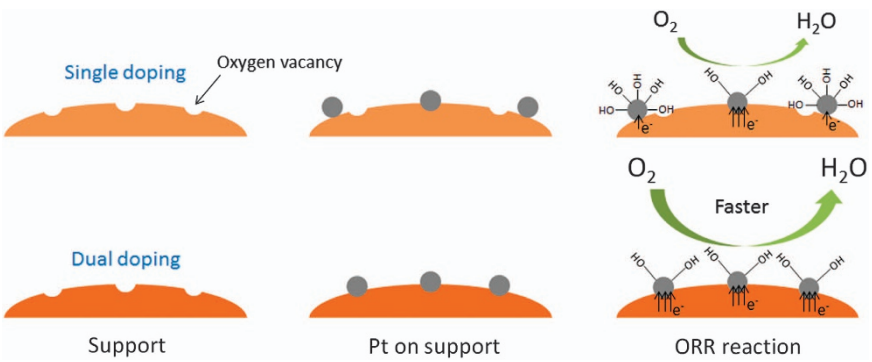

Figure 7 Schematic illustration of Pt loading on single-doped and dual-doped TiO_2 supports and the oxygen reduction reaction.

CONFLICT OF INTEREST

The authors declare no conflict of interest.

ACKNOWLEDGEMENTS

This work was supported by the Ministry of Science and Technology (MOST) (104-3113-E-011-002, 104-2923-M-011 -002 -MY3, 104-2911-I-011 -505 -MY2) and the Top University Projects of Ministry of Education (MOE) (100H451401). We acknowledge facility support from the National Synchrotron Radiation Research Center (NSRRC), Japan Synchrotron Radiation Research Institute (JASRI/SPring-8), Academic Sinica (106-0210-02-11-03) and National Taiwan University of Science and Technology (NTUST).

1 Lv, H. & Mu, S. Nano-ceramic support materials for low temperature fuel cell catalysts. *Nanoscale* **6**, 5063–5074 (2014).
2 Ho, V. T. T., Pillai, K. C., Chou, H.-L., Pan, C.-J., Rick, J., Su, W.-N., Hwang, B.-J., Lee, J.-F., Sheu, H.-S. & Chuang, W.-T. Robust non-carbon $Ti_{0.7}Ru_{0.3}O_2$ support with co-catalytic functionality for Pt: enhances catalytic activity and durability for fuel cells. *Energy Environ. Sci.* **4**, 4194 (2011).
3 Kim, K. W., Kim, S. M., Choi, S., Kim, J. & Lee, I. S. Electroless Pt deposition on Mn_3O_4 nanoparticles via the galvanic replacement process: electrocatalytic nanocomposite with enhanced performance for oxygen reduction reaction. *ACS Nano* **6**, 5122–5129 (2012).
4 Liu, Y. & Mustain, W. E. High stability, high activity Pt/ITO oxygen reduction electrocatalysts. *J. Am. Chem. Soc.* **135**, 530–533 (2013).
5 Jiang, Z.-Z., Wang, Z.-B., Chu, Y.-Y., Gu, D.-M. & Yin, G.-P. Ultrahigh stable carbon riveted Pt/TiO_2–C catalyst prepared by in situ carbonized glucose for proton exchange membrane fuel cell. *Energy Environ. Sci.* **4**, 728–735 (2011).
6 Ignaszak, A., Song, C., Zhu, W., Wang, Y.-J., Zhang, J., Bauer, A., Baker, R., Neburchilov, V., Ye, S. & Campbell, S. Carbon–$Nb_{0.07}Ti_{0.93}O_2$ composite supported Pt–Pd electrocatalysts for PEM fuel cell oxygen reduction reaction. *Electrochim. Acta* **75**, 220–228 (2012).
7 Du, Q., Wu, J. & Yang, H. Pt@Nb-TiO_2 catalyst membranes fabricated by electrospinning and atomic layer deposition. *ACS Catal.* **4**, 144–151 (2014).
8 Ho, V. T. T., Pan, C.-J., Rick, J., Su, W. i.-N. & Hwang, B.-J. Nanostructured $Ti_{0.7}Mo_{0.3}O_2$ support enhances electron transfer to Pt: high-performance catalyst for oxygen reduction reaction. *J. Am. Chem. Soc.* **133**, 11716–11724 (2011).
9 Tsai, M.-C., Nguyen, T.-T., Akalework, N. G., Pan, C.-J., Rick, J., Liao, Y.-F., Su, W.-N. & Hwang, B.-J. Interplay between molybdenum dopant and oxygen vacancies in a TiO_2 support enhances the oxygen reduction reaction. *ACS Catal.* **6**, 6551–6559 (2016).
10 Subban, C. V., Zhou, Q., Hu, A., Moylan, T. E., Wagner, F. T. & DiSalvo, F. J. Sol-gel synthesis, electrochemical characterization, and stability testing of $Ti_{0.7}W_{0.3}O_2$ nanoparticles for catalyst support applications in proton-exchange membrane fuel cells. *J. Am. Chem. Soc.* **132**, 17531–17536 (2010).
11 Kumar, A. & Ramani, V. Strong metal–support interactions enhance the activity and durability of platinum supported on tantalum-modified titanium dioxide electrocatalysts. *ACS Catal.* **4**, 1516–1525 (2014).
12 Ho, W., Yu, J. C. & Lee, S. Synthesis of hierarchical nanoporous F-doped TiO_2 spheres with visible light photocatalytic activity. *Chem. Commun.* 1115–1117 (2006).
13 Spadavecchia, F., Cappelletti, G., Ardizzone, S., Ceotto, M. & Falciola, L. Electronic structure of pure and N-doped TiO_2 nanocrystals by electrochemical experiments and first principles calculations. *J. Phys. Chem. C* **115**, 6381–6391 (2011).
14 Wang, J., Tafen, D. N., Lewis, J. P., Hong, Z., Manivannan, A., Zhi, M., Li, M. & Wu, N. Origin of photocatalytic activity of nitrogen-doped TiO_2 nanobelts. *J. Am. Chem. Soc.* **131**, 12290–12297 (2009).
15 Gong, J., Yang, C., Zhang, J. & Pu, W. Origin of photocatalytic activity of W/N-codoped TiO_2: H_2 production and DFT calculation with GGA+U. *Appl. Catal. B Environ.* **152–153**, 73–81 (2014).
16 Umare, S. S., Charanpahari, A. & Sasikala, R. Enhanced visible light photocatalytic activity of Ga, N and S codoped TiO_2 for degradation of Azo dye. *Mater. Chem. Phys.* **140**, 529–534 (2013).
17 Zhang, M., Wu, J., Lu, D. & Yang, J. Enhanced visible light photocatalytic activity for TiO_2 nanotube array films by codoping with tungsten and nitrogen. *Int. J. Photoenergy* **2013**, 1–8 (2013).
18 Sathish, M., Viswanathan, B., Viswanath, R. P. & Gopinath, C. S. Synthesis, characterization, electronic structure, and photocatalytic activity of nitrogen-doped TiO_2 nanocatalyst. *Chem. Mater.* **17**, 6349–6353 (2005).
19 Chisaka, M., Ishihara, A., Suito, K., Ota, K.-I. & Muramoto, H. Oxygen reduction reaction activity of nitrogen-doped titanium oxide in acid media. *Electrochim. Acta* **88**, 697–707 (2013).
20 Thind, S. S., Wu, G. & Chen, A. Synthesis of mesoporous nitrogen–tungsten co-doped TiO_2 photocatalysts with high visible light activity. *Appl. Catal. B Environ.* **111–112**, 38–45 (2012).
21 Carmo, M., dos Santos, A. R., Poco, J. G. R. & Linardi, M. Physical and electrochemical evaluation of commercial carbon black as electrocatalysts supports for DMFC applications. *J. Power Sources* **173**, 860–866 (2007).
22 Branko, N., Popov, D. L. H., Peterson, D. & Benjamin, T. Development of Ultra-Low Platinum Alloy Cathode Catalysts for PEM Fuel Cells. *DOE Hydrogen and Fuel Cells Program,* V153–V158 (2012).
23 Meier, J. C., Galeano, C., Katsounaros, I., Topalov, A. A., Kostka, A., Schüth, F. & Mayrhofer, K. J. J. Degradation mechanisms of Pt/C fuel cell catalysts under simulated start–stop conditions. *ACS Catal.* **2**, 832–843 (2012).
24 Huang, K., Sasaki, K., Adzic, R. R. & Xing, Y. Increasing Pt oxygen reduction reaction activity and durability with a carbon-doped TiO_2 nanocoating catalyst support. *J. Mater. Chem.* **22**, 16824 (2012).
25 Song, H., Jeong, T. G., Moon, Y. H., Chun, H. H., Chung, K. Y., Kim, H. S., Cho, B. W. & Kim, Y. T. Stabilization of oxygen-deficient structure for conducting $Li_4Ti_5O_{12}$-delta by molybdenum doping in a reducing atmosphere. *Sci. Rep.* **4**, 4350 (2014).

Supplementary Information accompanies the paper on the NPG Asia Materials website (http://www.nature.com/am)